Effect of surface roughness on self-assembled monolayer plasmonic ruler in nonlocal regime

Ghazal Hajisalem, Qiao Min, Ryan Gelfand, and Reuven Gordon

April 2014

This article was originally published at:

http://dx.doi.org/10.1364/OE.22.009604

Effect of surface roughness on self-assembled monolayer plasmonic ruler in nonlocal regime

Ghazal Hajisalem, Qiao Min, Ryan Gelfand, and Reuven Gordon*

Department of Electrical Engineering, University of Victoria, Victoria, British Columbia V8W 3P6, Canada
rgordon@uvic.ca

Abstract: Recently, self-assembled monolayers (SAMs) have been used for plasmonic rulers to measure the nonlocal influence on the Au nanoparticle - metal film resonance wavelength shift and probe the ultimate field enhancement. Here we examine the influence of surface roughness on this plasmonic ruler in the nonlocal regime by comparing plasmonic resonance shifts for as-deposited and for ultra-flat Au films. It is shown that the resonance shift is larger for ultra-flat films, suggesting that there is not the saturation from nonlocal effects previously reported for the spacer range from 0.7 nm to 1.6 nm. We attribute the previously reported saturation to the planarization of the as-deposited films by thinner SAMs, as measured here by atomic-force microscopy. This work is of interest both in probing the ultimate limits of plasmonic enhancement with SAMs for applications in Raman and nonlinear optics, but also in the study of SAM planarization as a function surface roughness.

OCIS codes: (240.6680) Surface plasmons; (250.5403) Plasmonics.

References and links

1. C. J. Orendorff, A. Gole, T. K. Sau, and C. J. Murphy, "Surface-enhanced Raman spectroscopy of self-assembled monolayers: Sandwich architecture and nanoparticle shape dependence," Anal. Chem. **77**(10), 3261–3266 (2005).
2. F. Le, D. W. Brandl, Y. A. Urzhumov, H. Wang, J. Kundu, N. J. Halas, J. Aizpurua, and P. Nordlander, "Metallic nanoparticle arrays: A common substrate for both surface-enhanced Raman scattering and surface-enhanced infrared absorption," ACS Nano **2**(4), 707–718 (2008).
3. J. Theiss, P. Pavaskar, P. M. Echternach, R. E. Muller, and S. B. Cronin, "Plasmonic nanoparticle arrays with nanometer separation for high-performance SERS substrates," Nano Lett. **10**(8), 2749–2754 (2010).
4. Q. Min, Y. Pang, D. J. Collins, N. A. Kuklev, K. Gottselig, D. W. Steuerman, and R. Gordon, "Substrate-based platform for boosting the surface-enhanced Raman of plasmonic nanoparticles," Opt. Express **19**(2), 1648–1655 (2011).
5. A. Ahmed and R. Gordon, "Directivity enhanced Raman spectroscopy using nanoantennas," Nano Lett. **11**(4), 1800–1803 (2011).
6. A. Ahmed and R. Gordon, "Single molecule directivity enhanced Raman scattering using nanoantennas," Nano Lett. **12**(5), 2625–2630 (2012).
7. X. Wen, Z. Xi, X. Jiao, W. Yu, G. Xue, D. Zhang, Y. Lu, P. Wang, S. Blair, and H. Ming, "Plasmonic coupling effect in Ag nanocap-nanohole pairs for surface-enhanced Raman scattering," Plasmonics **8**(2), 225–231 (2013).
8. W. Zhu, M. G. Banaee, D. Wang, Y. Chu, and K. B. Crozier, "Lithographically fabricated optical antennas with gaps well below 10 nm," Small **7**(13), 1761–1766 (2011).
9. T. Siegfried, Y. Ekinci, H. H. Solak, O. J. F. Martin, and H. Sigg, "Fabrication of sub-10 nm gap arrays over large areas for plasmonic sensors," Appl. Phys. Lett. **99**(26), 263302 (2011).
10. T. Siegfried, Y. Ekinci, O. J. F. Martin, and H. Sigg, "Gap plasmons and near-field enhancement in closely packed sub-10 nm gap resonators," Nano Lett. **13**(11), 5449–5453 (2013).
11. D. C. Marinica, A. K. Kazansky, P. Nordlander, J. Aizpurua, and A. G. Borisov, "Quantum plasmonics: Nonlinear effects in the field enhancement of a plasmonic nanoparticle dimer," Nano Lett. **12**(3), 1333–1339 (2012).
12. R. Fuchs and F. Claro, "Multipolar response of small metallic spheres: Nonlocal theory," Phys. Rev. B Condens. Matter **35**(8), 3722–3727 (1987).
13. C. David and F. J. García de Abajo, "Spatial nonlocality in the optical response of metal nanoparticles," J. Phys. Chem. C **115**(40), 19470–19475 (2011).

#208021 - $15.00 USD Received 10 Mar 2014; revised 2 Apr 2014; accepted 3 Apr 2014; published 15 Apr 2014

14. Q. Huang, F. Bao, and S. He, "Nonlocal effects in a hybrid plasmonic waveguide for nanoscale confinement," Opt. Express **21**(2), 1430–1439 (2013).
15. G. Toscano, S. Raza, A.-P. Jauho, N. A. Mortensen, and M. Wubs, "Modified field enhancement and extinction by plasmonic nanowire dimers due to nonlocal response," Opt. Express **20**(4), 4176–4188 (2012).
16. T. V. Teperik, P. Nordlander, J. Aizpurua, and A. G. Borisov, "Quantum effects and nonlocality in strongly coupled plasmonic nanowire dimers," Opt. Express **21**(22), 27306–27325 (2013).
17. T. V. Teperik, P. Nordlander, J. Aizpurua, and A. G. Borisov, "Robust subnanometric plasmon ruler by rescaling of the nonlocal optical response," Phys. Rev. Lett. **110**(26), 263901 (2013).
18. Y. Luo, A. I. Fernandez-Dominguez, A. Wiener, S. A. Maier, and J. B. Pendry, "Surface plasmons and nonlocality: A simple model," Phys. Rev. Lett. **111**(9), 093901 (2013).
19. L. Stella, P. Zhang, F. J. García-Vidal, A. Rubio, and P. García-González, "Performance of nonlocal optics when applied to plasmonic nanostructures," J. Phys. Chem. C **117**(17), 8941–8949 (2013).
20. J. Zuloaga, E. Prodan, and P. Nordlander, "Quantum description of the plasmon resonances of a nanoparticle dimer," Nano Lett. **9**(2), 887–891 (2009).
21. K. J. Savage, M. M. Hawkeye, R. Esteban, A. G. Borisov, J. Aizpurua, and J. J. Baumberg, "Revealing the quantum regime in tunnelling plasmonics," Nature **491**(7425), 574–577 (2012).
22. R. Esteban, A. G. Borisov, P. Nordlander, and J. Aizpurua, "Bridging quantum and classical plasmonics with a quantum-corrected model," Nat Commun. **3**, 825 (2012).
23. J. A. Scholl, A. García-Etxarri, A. L. Koh, and J. A. Dionne, "Observation of quantum tunneling between two plasmonic nanoparticles," Nano Lett. **13**(2), 564–569 (2013).
24. C. Sönnichsen, B. M. Reinhard, J. Liphardt, and A. P. Alivisatos, "A molecular ruler based on plasmon coupling of single gold and silver nanoparticles," Nat. Biotechnol. **23**(6), 741–745 (2005).
25. B. M. Reinhard, M. Siu, H. Agarwal, A. P. Alivisatos, and J. Liphardt, "Calibration of dynamic molecular rulers based on plasmon coupling between gold nanoparticles," Nano Lett. **5**(11), 2246–2252 (2005).
26. R. T. Hill, J. J. Mock, Y. Urzhumov, D. S. Sebba, S. J. Oldenburg, S.-Y. Chen, A. A. Lazarides, A. Chilkoti, and D. R. Smith, "Leveraging nanoscale plasmonic modes to achieve reproducible enhancement of light," Nano Lett. **10**(10), 4150–4154 (2010).
27. N. Liu, M. Hentschel, T. Weiss, A. P. Alivisatos, and H. Giessen, "Three-dimensional plasmon rulers," Science **332**(6036), 1407–1410 (2011).
28. R. T. Hill, J. J. Mock, A. Hucknall, S. D. Wolter, N. M. Jokerst, D. R. Smith, and A. Chilkoti, "Plasmon ruler with angstrom length resolution," ACS Nano **6**(10), 9237–9246 (2012).
29. J. J. Mock, R. T. Hill, Y.-J. Tsai, A. Chilkoti, and D. R. Smith, "Probing dynamically tunable localized surface plasmon resonances of film-coupled nanoparticles by evanescent wave excitation," Nano Lett. **12**(4), 1757–1764 (2012).
30. C. Ciracì, R. T. Hill, J. J. Mock, Y. Urzhumov, A. I. Fernández-Domínguez, S. A. Maier, J. B. Pendry, A. Chilkoti, and D. R. Smith, "Probing the ultimate limits of plasmonic enhancement," Science **337**(6098), 1072–1074 (2012).
31. M. D. Porter, T. B. Bright, D. L. Allara, and C. E. D. Chidsey, "Spontaneously organized molecular assemblies. 4. Structural characterization of n-alkyl thiol monolayers on gold by optical ellipsometry, infrared spectroscopy, and electrochemistry," J. Am. Chem. Soc. **109**(12), 3559–3568 (1987).
32. C. D. Bain, E. B. Troughton, Y. T. Tao, J. Evall, G. M. Whitesides, and R. G. Nuzzo, "Formation of monolayer films by the spontaneous assembly of organic thiols from solution onto gold," J. Am. Chem. Soc. **111**(1), 321–335 (1989).
33. A. Ulman, "Formation and structure of self-assembled monolayers," Chem. Rev. **96**(4), 1533–1554 (1996).
34. M. L. Wallwork, D. A. Smith, J. Zhang, J. Kirkham, and C. Robinson, "Complex chemical force titration behavior of amine-terminated self-assembled monolayers," Langmuir **17**(4), 1126–1131 (2001).
35. M. Godin, P. J. Williams, V. Tabard-Cossa, O. Laroche, L. Y. Beaulieu, R. B. Lennox, and P. Grütter, "Surface stress, kinetics, and structure of alkanethiol self-assembled monolayers," Langmuir **20**(17), 7090–7096 (2004).
36. J. C. Love, L. A. Estroff, J. K. Kriebel, R. G. Nuzzo, and G. M. Whitesides, "Self-assembled monolayers of thiolates on metals as a form of nanotechnology," Chem. Rev. **105**(4), 1103–1170 (2005).
37. A. I. Fernández-Domínguez, S. A. Maier, and J. B. Pendry, "Collection and concentration of light by touching spheres: A transformation optics approach," Phys. Rev. Lett. **105**(26), 266807 (2010).
38. P. Gupta, A. Ulman, S. Fanfan, A. Korniakov, and K. Loos, "Mixed self-assembled monolayers of alkanethiolates on ultrasmooth gold do not exhibit contact-angle hysteresis," J. Am. Chem. Soc. **127**(1), 4–5 (2005).
39. D. Stamou, D. Gourdon, M. Liley, N. A. Burnham, A. Kulik, H. Vogel, and C. Duschl, "Uniformly flat gold surfaces: Imaging the domain structure of organic monolayers using scanning force microscopy," Langmuir **13**(9), 2425–2428 (1997).
40. P. Nagpal, N. C. Lindquist, S.-H. Oh, and D. J. Norris, "Ultrasmooth patterned metals for plasmonics and metamaterials," Science **325**(5940), 594–597 (2009).
41. C. Ciracì, X. Chen, J. J. Mock, F. McGuire, X. Liu, S.-H. Oh, and D. R. Smith, "Film-coupled nanoparticles by atomic layer deposition: Comparison with organic spacing layers," Appl. Phys. Lett. **104**(2), 023109 (2014).
42. G. A. Cervantes Tellez, S. Hassan, R. N. Tait, P. Berini, and R. Gordon, "Atomically flat symmetric elliptical nanohole arrays in a gold film for ultrasensitive refractive index sensing," Lab Chip **13**(13), 2541–2546 (2013).

#208021 - $15.00 USD Received 10 Mar 2014; revised 2 Apr 2014; accepted 3 Apr 2014; published 15 Apr 2014

1. Introduction

Subwavelength gaps between metal nanostructures can be used to obtain high field localization for applications including surface-enhanced Raman scattering [1–7] and nonlinear optics [8–11]. There is great interest in determining the ultimate field enhancement, and how this is limited by nonlocal [12–19] and quantum effects [11, 20–23]. Recent works have sought to probe the ultimate limits of field enhancement in such subwavelength gaps by using the concept of plasmonic rulers [17, 24–30]. Those works used SAMs to create a gap between a metal film and gold nanoparticles (NPs) [28–36]. For the smallest length SAMs, however, the surface roughness was comparable to the length of the SAM itself; therefore, the gap distance was sensitive to the way in which the SAMs assembled on the metal film. This is particularly important because nonlocal saturation arises for the gaps corresponding to the shorter SAMs, for gaps between 0.5 nm and 1.5 nm [28–30, 37–41].

In this work, we investigate the influence of surface roughness on the plasmonic scattering spectral peak shifts of NPs on SAMs, both on ultra-flat and on as-deposited metal films. Larger shifts are seen for the ultra-flat films, suggesting that there is not the saturation from nonlocal effects that was previously reported. In addition, atomic-force microscope (AFM) studies reveal that there is significant planarization from the SAMs on the as-deposited films, which means that the mean separation between the NPs and the metal films is increased on average and gives the impression of saturation if not considered.

2. Fabrication

To fabricate as-deposited samples, 30 nm of Au was deposited at rate of 1 Å/s and at an elevated temperature of 200 °C onto a cleaned cover slide glass by an electron beam and thermal evaporator (Angstrom Engineering Glove-box Evaporator). A 5 nm chromium film, deposited at 1 Å/s, was used as an adhesion layer. This is similar to the procedure of past works [28, 30]; however, we used a lower evaporation rate and elevated temperature.

Ultra-flat samples were prepared by depositing a 30 nm Au film onto silicon wafers at a rate of 1 Å/s and temperature of 200 °C. Promptly after evaporation, the Au slides were coated with a thin layer of optical epoxy (Norland Optical Adhesive 61) followed by a cleaned glass slide. The optical epoxy was used as adhesion layer between the Au film and the glass slide, and it was cured by exposing to UV light for 5 min. Then the Au film on epoxy on glass slide was "stripped" off from the Si wafer, revealing the ultra-flat surface of Au film [42].

SAMs of amine-terminated alkanethiols were prepared on the fresh as-deposited and ultra-flat Au films as a spacer layer in the nonlocal regime. The thickness of the spacer layer depends on the number of carbons in the alkanethiol, providing a spacer distance between 0.7 nm and 1.6 nm. Here we used 3-amino-1-propanethiol hydrochloride (739294, Sigma-Aldrich), 6-amino-1-hexanethiol hydrochloride (733679, Sigma-Aldrich), and 11-amino-1-undecanethiol hydrochloride (674397, Sigma-Aldrich) (referred to as "c3", "c6", and "c11"). 2 mM solutions of the amine-terminated alkanethiols were prepared in absolute ethanol in cleaned glass containers. SAMs were fabricated by immersing an Au film substrate into a thiol container for 18 hours, followed by sonicating the substrate for 2 minutes. The Au film substrate was rinsed with absolute ethanol for 15 seconds. The process of sonication and rinsing was repeated four times for each sample. Finally, all substrates were dried using pure nitrogen gas [28, 30].

Following a past work [30], 60 nm NPs (742015, Sigma-Aldrich) were immobilized electrostatically on top of the SAMs by incubating with 500 µl of the colloidal stock for 30 min followed by rinsing with deionized water (USF Elga, Maxima, model Scientific MK3, 18.2 MΩ-cm) for 15 second and drying with a stream of pure nitrogen gas.

#208021 - $15.00 USD Received 10 Mar 2014; revised 2 Apr 2014; accepted 3 Apr 2014; published 15 Apr 2014

3. Roughness measurements

An AFM (Agilent 5500) was used to measure the roughness of the as-deposited and ultra-flat samples within a 4 μm × 4 μm scanning area. Figures 1, 2 and 3 show representative AFM scans for different samples. Slowly-varying long scale roughness of the order of microns was subtracted from the data using roughness analysis of the software Gwyddion (Version 2.34). Figure 1 shows that the surface roughness from commercial gold samples (EMF Corp.) is 2 nm, whereas our as-deposited gold films have a surface roughness of 1 nm and the template-stripped gold films have a surface roughness of 0.1 nm. Figure 2 shows the surface roughness for as-deposited films for different SAM layers. Figure 3 shows the surface roughness for template stripped films for different SAM layers.

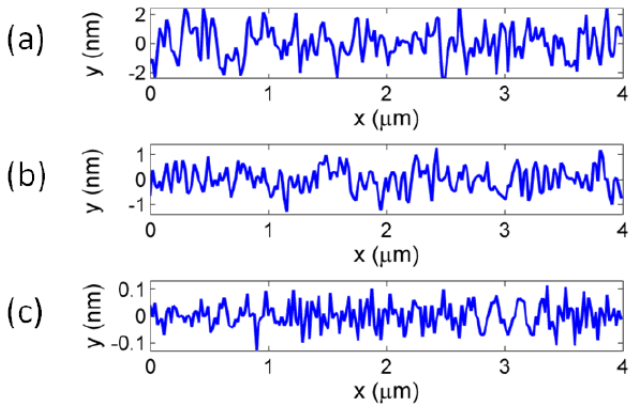

Fig. 1. Representative surface height scans using AFM for Au film. (a) Height profile of a bare commercial Au slide is shown for reference (100 nm thickness, EMF Corp.) with greater roughness than our as-deposited films. (b) Bare as-deposited 30 nm Au film. (c) Bare ultra-flat 30 nm Au film fabricated by template stripping.

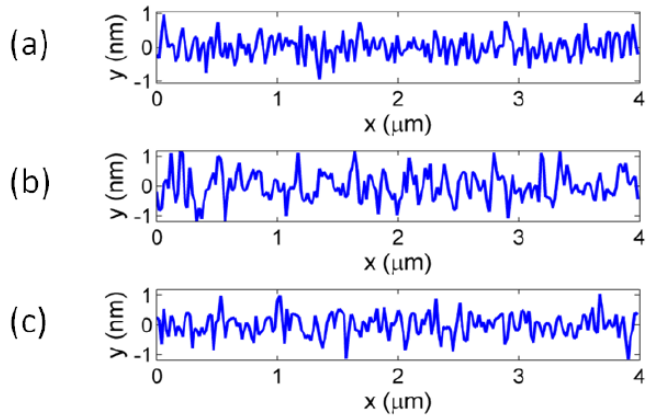

Fig. 2. Representative surface height scans using AFM for SAMs of amine-terminated alkanethiols with different alkane carbon chain length on as-deposited Au films. (a) c3, (b) c6 and (c) c11.

#208021 - $15.00 USD Received 10 Mar 2014; revised 2 Apr 2014; accepted 3 Apr 2014; published 15 Apr 2014

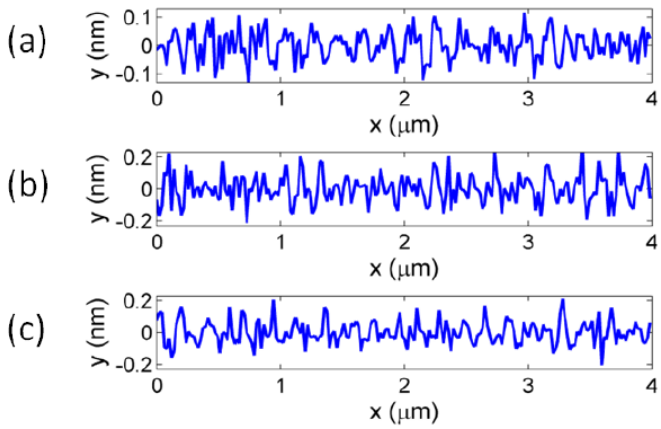

Fig. 3. Representative surface height scans using AFM for varying SAMs on ultra-flat Au films. (a) c3, (b) c6 and (c) c11.

Figure 4 shows the average root mean square (RMS) roughness of bare as-deposited and ultra-flat Au films (referred to as "c0") and for films with SAMs. For each sample, the standard deviation was obtained from more than 15 measurements at different locations on a sample. The average RMS roughness of the bare ultra-flat Au film was 0.05 nm, while the RMS of the bare as-deposited film was 0.5 nm. From these measurements, we see that the SAMs planarized the as-deposited Au significantly, particularly for the c3 case, where the SAMs chain is 0.7 nm (at 30° tilt) [28] and the surface roughness is 0.5 nm (comparable). A slight increase in roughness is observed for SAMs on ultra-flat samples and this is believed to be due to disorder of the SAMs.

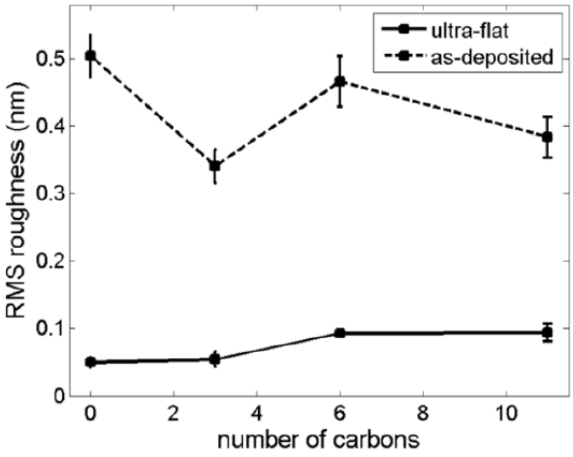

Fig. 4. AFM measured surface roughness for bare Au and Au with SAMs. Ultra-flat and as-deposited Au films are shown.

4. Dark field scattering

Figure 5(a) shows a schematic of the dark-field (DF) scattering measurement setup. A collimated white light (LS-1-LL, Ocean Optics Inc.) source was focused onto the sample by a 20 × microscope objective (0.42 NA, Mitutoyo Plan Apo) at 70° to the surface normal. The off-normal excitation is used to excite the localized surface plasmon resonance of the NP-metal film [28, 29]. The scattered light from the NP-metal film was collected at 15° relative to the normal of the sample by a 40 × microscope objective (0.68 NA, Zeiss). The scattered beam was split into two beams passing through a 50-50 beam splitter. One path was directed

#208021 - $15.00 USD Received 10 Mar 2014; revised 2 Apr 2014; accepted 3 Apr 2014; published 15 Apr 2014

into a CCD camera (GC660, Allied Vision Technologies) to take the DF scattering image (Fig. 5(b)). The other path was directed into a spectrometer (QE65000, Ocean Optics Inc.) to take the scattering spectrum of the sample from the same spot as the DF scattering image (Fig. 5(c)). Care was taken to avoid regions with spurious scatterers (e.g., from aggregates or dimers) that showed distinguishable changes in the DF image and spectrum. The DF scattering image shows a good distribution of nanoparticles (i.e., not aggregated or too sparse).

Figure 5(d) shows the evolution of the normalized plasmonic scattering spectral peak as a function of the carbon number. For each sample, the standard deviation in the resonance wavelength was obtained from more than 15 measurements at different locations on a sample. We also present the data digitized from Ref. 30, which is seen to be consistent with the measurements on our as-deposited films.

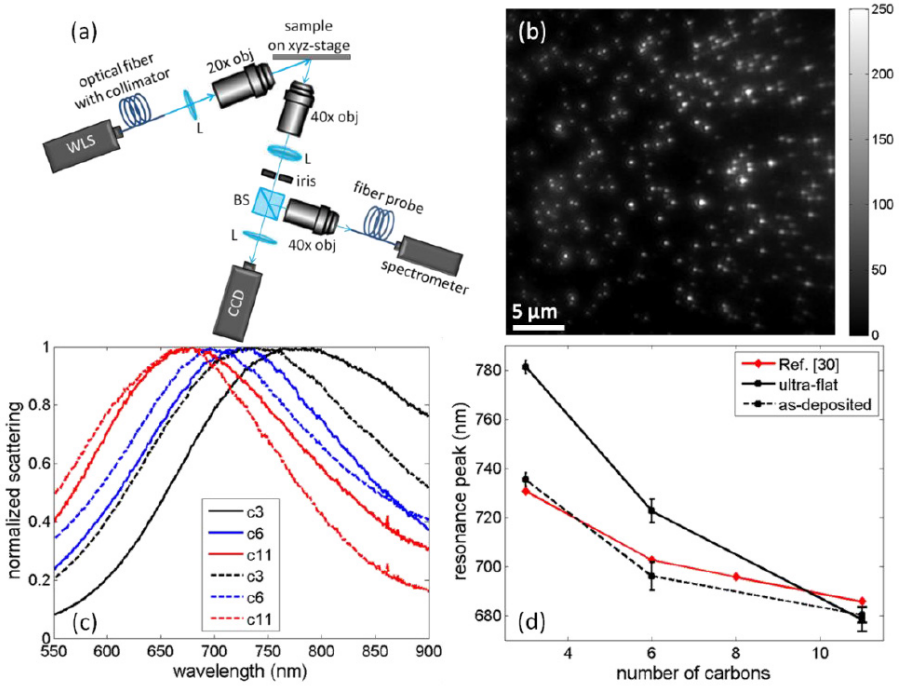

Fig. 5. (a) Optical configuration for the scattering measurements of NPs on metal films. WLS = white light source, L = lens, obj = microscope objective lens, BS = beam splitter. (b) DF scattering image of NPs deposited on the ultra-flat film with 6-amino-1-hexanethiol SAM. The color bar represents the CCD's digital output. (c) Normalized scattering spectra of NPs deposited on ultra-flat Au films (solid lines) and on as-deposited Au films (dashed lines) for SAMs with different numbers of carbon. (d) Summary of peak positions of plasmonic scattering as a function of the number of carbons including experimental data from Ref. 30 on as-deposited metal films.

5. Discussion

To understand why the ultra-flat film shows a larger plasmonic resonance shift than the as-deposited films, we consider the influence of planarization of the SAMs on the as-deposited films. Figure 6(a) shows a schematic of planarization, where h_0 is the SAM's theoretical height [28] (c3, c6 and c11 SAM layers heights of 0.69 nm, 0.94 nm and 1.55 nm), Δh is the surface roughness of the Au film, $\Delta h'$ is the roughness with the SAM, and the degree of planarization is defined as $(\Delta h - \Delta h')/\Delta h$.

#208021 - $15.00 USD Received 10 Mar 2014; revised 2 Apr 2014; accepted 3 Apr 2014; published 15 Apr 2014

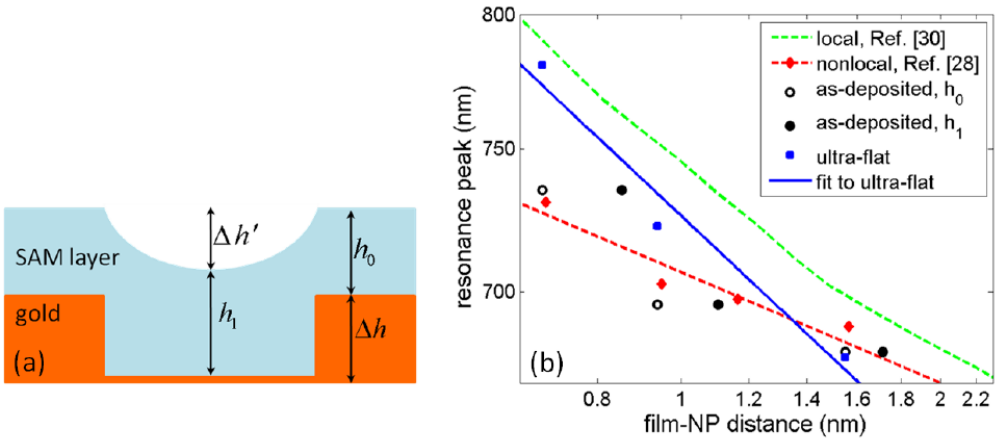

Fig. 6. (a) Schematic showing the planarization – note this is meant to represent random surface roughness and is not for a periodic film. h_0 is the SAM's theoretical height (30° tilted) [28], Δh is the surface roughness of the Au film, $\Delta h'$ is the surface roughness with SAMs, h_1 is the maximum film-NP distance. (b) Dark-field scattering resonance wavelength as a function of the NP-film distance. Experimental data from Ref. 28 using the theoretical SAM height is also shown. Considering planarization, maximum and minimum thicknesses are shown for as-deposited Au films. Straight line fits on log-log scale are shown. Also shown is the local response theory digitized from Ref. 30.

Considering this planarization, we plot the minimum separation between NPs and the metal film (h_0) and the maximum (h_1) for the film separation in Fig. 6(b). We see that the as-deposited results are comparable with the ultra-flat results, so long as the planarization is considered. This shows that the planarization of the SAMs plays an important role in the observed plasmonic resonances and should be considered.

Using the Lindhard dielectric and the Fermi velocity of Au, it is expected that the β factor for nonlocality is 1.06×10^6 m/s. The best-fit beta found in a past work was 1.27×10^6 m/s [30], which gives significant saturation for gap sizes below 1 nm. Recent comparisons with time-dependent density functional theory suggest that screening effects actually create effectively smaller gaps (so long as tunneling is neglected), which is the opposite trend to the expected saturation of the nonlocal hydrodynamic model [11, 16, 17]. Here we observe that much less saturation is seen for the ultra-flat films, and the trend follows quite closely to local calculations; that is, there is no saturation seen in our work for the range of 0.7 nm to 1.6 nm. For gap sizes below 0.7 nm, tunneling is expected to play a role, which is not captured by the usual non-local hydrodynamic model [17].

6. Conclusion

We have studied the influence of surface roughness in probing the ultimate limits of the plasmonic response using SAM spacers. These results do not show the saturation reported previously for SAM layers between 0.7 nm and 1.6 nm. We attribute those past results to the planarization of the as-deposited gold films by the SAMs. These results are of interest to the future study of plasmonic systems using SAMs to achieve gaps with high field enhancements, for example in the area of SERS [1–7] or nonlinear optics [12–19].

Acknowledgments

This work is funded by an NSERC Strategic Project Grant.

#208021 - $15.00 USD Received 10 Mar 2014; revised 2 Apr 2014; accepted 3 Apr 2014; published 15 Apr 2014